MECHANICAL RESPONSE OF THICK LAMINATED BEAMS AND PLATES SUBJECT TO OUT-OF-PLANE LOADING

C. C. Hiel, Research Scientist

Engineering Science and Mechanics Department

H. F. Brinson, Professor

Engineering Science and Mechanics Department

Support for this work was provided by

NASA-Ames Research Center under Contract No. NCC-2-71

ABSTRACT

The paper demonstrates the use of simplified elasticity solutions to determine the mechanical response of thick laminated beams and plates subject to out-of-plane loading.

Excellent results were obtained which compare very favorably with theoretical numerical and experimental analysis from other sources.

The most important characteristic of the solution methodology presented is that it combines great mathematical precision with simplicity. This symbiosis has been sorely needed for design with advanced composite materials.

KEYWORDS: Laminated beam, laminated plate bending, simplified elasticity solution

1. Introduction

The number of applications for which polymer based composites are used is increasing every year. Projections for the last decade of our century indicate that structures will be composed of between 25% and 50% of composite materials depending on the industrial sector for which they are designed and built. The latest developments in the areas of processing and manufacturing technology open such a broad avenue of new possibilities that the use of composites, by the end of the nineties, will probably be even higher than the most optimistic predictions.

With this increasing number of applications, at least two problems become more and more urgent:

a) How to properly design with composites

b) How to ensure the durability of components subject to mechanical and environmental loading conditions

The classical laminated plate theories (CPT) are inadequate for design especially in those applications where out of plane loads need to be supported, i.e., bending, buckling, impact etc. The shear-deformation effects are unaccounted for in the CPT which in turn leads to incorrect estimates of durability.

The objective of this paper is to demonstrate the use of a simplified theory of elasticity approach for the stress analysis of laminated beams and plates. The advantage of this solution methodology is that closed form analytical solutions can be obtained for any laminate layup. In addition, factors which are related to the durability such as resin rich regions, gradients in material properties due to processing of thick laminates, etc. can be incorporated without undue complications.

The theory of elasticity for laminated beams and plates is based on an approach which has been advocated by Biot [1,2]. The accuracy of the resulting solutions to determine the deflections, stresses and strains in multilayered components is demonstrated. Results are compared with existing elasticity solutions, experiments and finite element results.

The ability to use analytical solutions which are simple, accurate and which can incorporate realistic fabrication features should greatly enhance the engineers ability to design durable and trouble-free laminated components.

2. Formulation of the Problem

We consider an elastic and orthotropic plate of thickness h, described by the displacement components u and w. The x-axis is directed along the span and the z-axis is perpendicular to the plate, as shown in Fig. 1. The strain components are:

$$\varepsilon_x = \frac{\partial u}{\partial x} \, , \quad \varepsilon_z = \frac{\partial w}{\partial z} \, , \quad \varepsilon_{xz} = \frac{1}{2} \left(\frac{\partial u}{\partial z} + \frac{\partial w}{\partial x} \right) \tag{1}$$

The stress-strain relations for the orthotropic material are:

$$\begin{aligned} \sigma_x &= C_{11} \, \varepsilon_x + C_{13} \, \varepsilon_z \\ \sigma_z &= C_{13} \, \varepsilon_x + C_{33} \, \varepsilon_z \\ \tau_{xz} &= 2C_{55} \, \varepsilon_{xz} \end{aligned} \tag{2}$$

in which

$$\begin{aligned} C_{11} &= (1 - \nu_{23}^2 \, E_{33}/E_{22}) \, E_{11}/V \\ C_{13} &= (\nu_{13} + \nu_{12} + \nu_{23}) \, E_{33}/V \\ C_{33} &= (1 - \nu_{13}^2 \, E_{33}/E_{11}) \, E_{22}/V \end{aligned} \tag{3}$$

$$C_{55} = G_{13}$$

$$V = [1 - \nu_{12}(\nu_{12}\, E_{22}/E_{11} + 2\nu_{23}\, \nu_{13}\, E_{33}/E_{11}) - \nu_{13}^2\, E_{33}/E_{11} - \nu_{23}^2\, E_{33}/E_{22}] \tag{4}$$

If the stress σ_z, normal to the plate, is neglected and assumed to be zero, then relocations (2) can be rearranged and become,

$$\sigma_x = 4M\, \varepsilon_x \tag{5}$$
$$\tau_{xz} = 2\, G_{13}\, \varepsilon_{xz}$$

The coefficient M can be written as:

$$M = \frac{1}{4C_{33}} (C_{11}\, C_{33} - C_{13}^2) \tag{6}$$

Substituting the relations (3) into (6), we obtain

$$M = \frac{E_{11}}{4(1 - \nu_{13}\, \nu_{31})} \tag{7}$$

and for an isotropic material;

$$M = \frac{E}{4(1-\nu^2)} \tag{8}$$

The equilibrium equations are:

$$\frac{\partial \sigma_x}{\partial x} + \frac{\partial \tau_{xz}}{\partial z} = 0$$

$$\frac{\partial \tau_{xz}}{\partial x} + \frac{\partial \sigma_z}{\partial z} = 0 \qquad (9)$$

Note that the assumption $\sigma_z = 0$ is only introduced in the stress-strain relations and not in the equilibrium equations. This is due to the fact that we can neglect the magnitude of σ_z with respect to σ_x and τ_{xz} but not its spatial rate of change. We investigate displacement fields, which are sinusoidally distributed along x. Trial solutions for u and w can be written as:

$$u = U(z) \sin (\ell x) \qquad (10)$$

$$w = W \cos (\ell x)$$

In which ℓ is the wavelength along the x-direction. An additional approximation is introduced here by assuming W to be a constant, equal to the average displacement across the thickness. The second equation (3) yields

$$\tau_{xz} = \tau(z) \sin \ell x$$

$$\text{with } \tau(z) = G_{13} \left(\frac{dU}{dz} - \ell w\right)$$

By eliminating σ_x and U between equations (3) and the first of equations (9). We btain the following differential equation in τ_{xz} .

$$\frac{d}{dz} \left(\frac{1}{4M} \frac{d\tau_{xz}}{dz}\right) - \frac{\ell^2 \tau_{xz}}{G_{13}} = \ell^3 w \qquad (12)$$

The integration of this second-order differential equation in τ_{xz} requires two boundary conditions. Let the boundaries of the beam be located at $z = \pm h/2$ (Fig. 1) and assume the shear $\tau_1 = \tau_{xz}\ (h/2)$ and $\tau_2 = \tau_{xz}\ (-h/2)$ to be given at the top and bottom. With these boundary conditions the function $\tau_{xz}(z)$ is obtained by integration of Eq. 12, where M, G_{13}, ℓ and w play the role of parameters. By integrating the second equilibrium equation (9) along z, we obtain:

$$q = -\int_{-h/2}^{h/2} \tau_{xz}\, dz \tag{13}$$

The total load applied to the same unit area is:

$$[\sigma_z]_1 = [\sigma_z]_2 = q \cos \ell x \tag{14}$$

Since $\tau(z)$ is known in terms of w, equation (13) determines the deflection w when the load q is given when we know τ_{xz}, the values of U and σ_x are determined by combining the first of equations (1) with the first of equations (3). We obtain:

$$U = \frac{1}{4M\ell^2} \frac{d\tau_{xz}}{dz} \tag{15}$$

$$\sigma_x = \frac{1}{\ell} \frac{d\tau_{xz}}{dz} \cos \ell x \tag{16}$$

3. Solution for Lamina and Laminates

The foregoing methodology may be used to analyze laminates constituted by the superposition of adherent homogeneous layers.

Consider first a single-orthotropic lamina of thickness h and constant elastic coefficients G_{13} and M. The shear stresses at the top and bottom of the lamina are denoted by τ_1 and τ_2 respectively.

Eqn. 12 is readily integrated in this case, the solution of which is

$$\tau_{xz} = C_1 \cosh\beta\ell z + C_2 \sinh\beta\ell z - \ell G_{13} W \tag{17}$$

with

$$C_1 = \left[\frac{1}{2}(\tau_1 + \tau_2) + \ell G_{13} W\right] \frac{1}{\cosh\beta\gamma}$$

$$C_2 = \frac{1}{2}(\tau_z - \tau_2) \frac{1}{\sinh\beta\gamma}$$

$$\gamma = \frac{1}{2}\ell h$$

$$\beta = 2\sqrt{\frac{M}{G_{13}}}$$

From equation (15) we derive the values U_1 and U_2 of U at the top and bottom of the layer

$$U_1 = \frac{1}{4\sqrt{MG_{13}}}(\tau_1 a + \tau_2 b) + cW$$

$$U_2 = \frac{1}{4\sqrt{MG_{13}}}(\tau_1 b + \tau_2 a) - cW \tag{18}$$

with

$$a = \tanh\beta\gamma + \frac{1}{\tanh\beta\gamma}$$

$$b = \tanh\beta\gamma - \frac{1}{\tanh\beta\gamma}$$

$$c = \frac{1}{\beta}\tanh\beta\gamma$$

The normal load $q\cos\ell x$ applied to this layer is obtained from Eq. 13.

$$q = -(\tau_1 + \tau_2)\, C + \ell^2 h\, G_{13}\, W\left(1 - \frac{C}{\gamma}\right) \tag{19}$$

For a laminate constituted of N adhering layers, the i-th layer of thickness h_i is characterized by the material properties $(\bar{G}^i_{13})$ and $(\bar{M}^i)$. Corresponding parameters are a_i, b_i and c_i. We denote by τ_i and τ_{i+1} the shear stresses at the top and bottom of the i-th layer respectively and by U_i and U_{i+1} the displacements at the corresponding faces. The condition of adherence of the layers i and i+1 are obtained by equating the displacements at the interface. Applying equations (18), we obtain a recurrency equation which has to be satisfied by the interface stress at three subsequent interfaces.

$$B_i\,\tau_i + (A_i + A_{i+1})\,\tau_{i+1} + B_{i+1}\,\tau_{i=2} = -(C_i + C_{i+1})\,\ell W \tag{20}$$

where $$A_i = \frac{a_i}{4\sqrt{\bar{M}^i\, G^i_{13}}} \qquad i = 1,2 \ldots N$$

$$B_i = \frac{b_i}{4\sqrt{\bar{M}^i\, \bar{G}^i_{13}}}$$

$$\bar{G}^i_{13} = \frac{G_{LT}\, G_{TT}}{G_{LT}\sin^2\theta + G_{TT}\cos^2\theta} \qquad \text{layer \# i} \tag{21}$$

$$\bar{M}^i = \frac{\bar{E}_{11}}{4(1 - \bar{\nu}_{13}^2 \frac{ET}{\bar{E}_{11}})} \qquad \text{layer \# i} \tag{22}$$

with:

$$\bar{E}_{11} = \frac{1}{\frac{\cos^2\theta}{E_L} + (\frac{1}{G_{LT}} - \frac{2\nu LT}{EL}) \sin^2\theta \cos^2\theta + \frac{\sin^2\theta}{E_T}}$$

$$\bar{\nu}_{13} = \bar{E}_{11}[\frac{\nu_{LT}}{E_L} (\sin^4\theta + \cos^4\theta) -$$

$$(\frac{1}{E_L} + \frac{1}{E_T} - \frac{1}{G_{LT}}) \sin^2\theta \cos^2\theta]$$

note: for $\theta = 0$ $\quad \bar{G}_{13} = G_{LT} = G_{13}$

$$\bar{E}_{11} = E_L = E_{11}$$

$$\bar{\nu}_{13} = \nu_{LT} = \nu_{13}$$

Thus $\quad M = \frac{E_{11}}{4(1 - \nu_{13}^2 \frac{E_2}{E_1})}$

for $\theta = 90^o$ $\quad \bar{G}_{13} = G_{TT} = G_{23}$

$$\bar{E}_{11} = E_T = E_{22}$$

$$\bar{\nu}_{13} = \nu_{LT} \frac{E_T}{E_L} = \nu_{13} \frac{E_{22}}{E_{11}}$$

Thus $\quad M = \frac{E_{22}}{4(1 - \nu_{13}^2 \frac{E_2}{E_1})}$

in which θ is the angle between the fibers (which are oriented in the x-y plane) and the x-direction.

Eqn. 20 is a system of (n-1) equations, in the (n-1) interface stresses. Assuming that the interface stresses τ_1 and τ_n at the top and bottom of the laminate are given. The other interface stresses are obtained in terms of a single unknown W. The latter is evaluated by considering the total load of q cos ℓx applied to the laminate. It is the sum of all individual loads of cos ℓx acting on each layer, Hence

$$q = \sum^{i} q_i \tag{23}$$

where according to Eq. 19

$$q_i = -(\tau_i + \tau_{i+1})\, c_i + \ell^2 h_i\, G^i_{xz}\,(1 - \frac{C_i}{\gamma_i})\, W \tag{24}$$

we may write

$$q = -\sum^{i} (\tau_i\ \tau_{i+1})\, C_i + \ell^2 W \sum^{i} h_i\, \bar{G}^i_{13}(1 - \frac{C_i}{\gamma_i} \tag{25}$$

Since τ_i is a known function of W, while q is given, equation (25) determines W.

Equations (13 ... 21) thus allow us to obtain closed form analytical solutions for any laminate layup. These solutions can easily be programmed on a hand calculator or PC and be used in the design office for preliminary sizing of laminated composite beams and sandwich panels.

In the remainder of this paper, we will demonstrate the use and the accuracy of this approach. Results are compared with theoretical, numerical and experimental data which is available in the literature.

4. Results for Lamina with 0° and 90° Orientation

We shall first illustrate that well-known strength of materials results can be retrieved or a special case of the elastcity solution which we outlined in 3.

Consider the case of a simply supported homogeneous orthotropic beam subject to three point bending. The conditions at the top and bottom surface are $\tau_1 = 0$ and $\tau_2 = 0$, as schematically indicated in Fig. 2.

Upon substitution of τ_1 and τ_2 in Eq. 19, we obtain

$$q = \ell^2 h\, \bar{G}_{13} \left(1 - \frac{\tanh \beta\gamma}{\beta\gamma}\right) w \tag{26}$$

$$\text{or } W = \frac{q}{\ell^2 h\, \bar{G}_{13} \left(1 - \frac{\tanh \beta\gamma}{\beta\gamma}\right)} \tag{27}$$

The deflection of a beam on three-point bending is easily found by expanding the load P in Fourier series and by adding the corresponding displacement components. The result is:

$$W = \frac{2P}{a\ell^2 h \bar{G}_{13}} \sum_{1,3,5}^{\infty} \left(1 - \frac{1}{\dfrac{(1 - \tanh \beta\gamma_m)}{\beta\gamma_m}}\right) \tag{28}$$

$$\text{with } \gamma_m = m \frac{\pi h}{2a}$$

Expanding $\tanh \beta\gamma_m$ in series, and retaining the first three terms, we obtain

$$W = \frac{P\bar{E}_{11}}{2\frac{a}{h}(\bar{G}_{13})^2} \sum_{1,3,5} \frac{1}{\frac{1}{3}(\beta\gamma_m)^4 [1 - \frac{6}{15}(\beta\gamma_m)^2]} \tag{29}$$

using the binomial approximation

$$\frac{1}{1 - \frac{6}{15}(\beta\gamma_m)^2} = 1 + \frac{6}{15}(\beta\gamma_m)^2 \tag{30}$$

we obtain, by adding the three terms

$$W = \frac{Pa^3}{48\,\bar{E}_{11}\,I}\left[.9994 + 1.12\,\frac{\bar{E}_{11}}{\bar{G}_{13}}\left(\frac{h}{a}\right)^2\right] \tag{31}$$

This is a well-known result, from the theory of strength of materials, that is often used to obtain the interlaminar shear modulus ($\bar{G}_{13}$) from short beam deflection data.

The difference (in %) between the deflection obtained using the elasticity solution (Eq. 28) and the strength of materials result Eq. 31) is plotted in Fig. 3. The curves are representative for a undirectional graphite epoxy with $\bar{E}_{11} = E_{11} = 171$ Gp$_a$ (25 10^6 psi) and $\bar{G}_{13} = G_{13} = 1.37$ Gpa (.210 psi) . The difference is calculated as:

$$\text{DIFF} = \frac{W\ (\text{Eq. } 31) - W\ (\text{Eq. } 28)}{W\ (\text{Eq. } 28)} \times 100\% \tag{32}$$

Fig. 3 indicates that the strength of materials solution slightly overestimates the deflection (less than 2%) for ratio's of beam-span to thickness which are larger than 10. Both solutions deviate rapidly for

span to thickness ratio's which are less than 4. We can thus conclude that the strength of materials formula (Eq. 21) is a good approximation for all practical purposes.

Unfortunately simple equations as Eq. 31 are not available for laminates: Nevertheless in 5 we will present actual solutions obtained, using the methodology outlined in 4. These solutions represent an excellent compromise between precision and flexibility as will be shown.

5. Results for Laminates

5.1 Cylindrical Bending of a 0°/90°/0° Laminate

The solution methodology for a laminate is first applied to a 0°/90°/0° subject to cylindrical bending, as schematically shown in Fig. 4. The results obtained are compared with these which were published by Pagano [3] who rigorously solved this elasticity problem (i.e. without bringing in the assumption that σ_z is much smaller than σ_x and τ_{xz}).

First Eq.'s 20 are solved for the shear stresses at the 0°/90° interfaces. Upon substitution of these results into Eq. 25, the center deflection is obtained as

$$W = \frac{q}{\ell\left[\frac{a_1}{\sqrt{M_1 G_{13}}} + \frac{2\beta_2 C_2}{\sqrt{M_2 G_{23}}} + 2\ell h_1 G_{13}\left(1 - \frac{C_1}{2\gamma_1}\right) + \ell h_2 G_{23}\left(1 - \frac{C_2}{\gamma_2}\right)\right]}$$

where coefficients a_i, b_i and c_i are defined in Eq. 18 and M_1 and M_2 are defined by substituting $\theta = 0°$ and $90°$ into Eq. 22. The same substitution into Eq. 21 defines $G_{13} = G_{LT}$ and $G_{23} = G_{TT}$.

The numerical values used Pagano's elasticity solution are:

$$E_{11} = 171 \text{ GPa } (25\ 10^6 \text{ psi})$$
$$E_{22} = 6.85 \text{ GPa } (10^6 \text{ psi})$$
$$G_{13} = 3.42 \text{ GPa } (.510^6 \text{ psi})$$
$$G_{23} = 1.37 \text{ GPa } (.210^6 \text{ psi})$$

The plate has unit thickness, consequently $h_1 = h_2 = \frac{1}{3}$ (as indicated in Fig. 4).

In order to compare our results with Pagano's [3]. We need to multiply the deflections, obtained from Eq. 33, with a normalization factor:

$$\bar{W} = W \frac{100\ E_{22}(h_2 + 2h_1)^3}{q_o a^4} \tag{34}$$

The value $\bar{W}$ is obtained for different span to thickness ratio's (a/h) and represented by the solid line in Fig. 5. The circles are the $\bar{W}$ values which were obtained, using the much more cumbersome Pagano solution. As can be seen, the agreement is excellent. Eq. 33 is thus especially useful as a simple solution for short thick beams (as used for composite leaf springs, hinges, helicopter rotor-connections and many other primary loadbearing structural applications). Fig 5 also indicates that our solution for $\bar{W}$ correctly converges towards the classical plate theory (CPT) solutions for large span to thickness ratios.

The shear stress τ_2 was solved, from Eq's 20, as:

$$\tau_2 = AW\ell \tag{35}$$

$$\text{with } A = -\frac{4(C_1 + C_2)}{\frac{a_1}{\sqrt{M_1 G_{13}}} + \frac{2 \beta_2 C_2}{\sqrt{M_2 G_{23}}}} \tag{35}$$

To obtain this solution for τ_2 we made use of the symmetry of the laminate, with respect to the x-axis, thus $\tau_2 = \tau_3$ and $\tau_1 = \tau_4 = 0$.

After substitution of Eq. 35 into Eq. 17, we obtain the shear stress distribution in the 0° layer (layer 1)

$$\tau_{xz} = C_1 \cosh\beta_1 \ell z + C_2 \sinh\beta_2 \ell z - \ell G_{13} W$$

$$\text{with } C_1 = [\tfrac{1}{2} A + G_{13}] \frac{\ell w}{\cosh \beta_1 \gamma_1} \tag{36}$$

$$C_2 = -\frac{1}{2} \frac{A \ell w}{\sinh \beta_1 \gamma_1}$$

The shear stress distribution in the 90° layer (layer 2) is obtained as

$$\tau_{xz} = C_1 \cosh\beta_2 \ell z - \ell G_{23} W$$

$$\text{with } C_1 = (A + G_{23}) \frac{\ell w}{\cosh \beta_2 \gamma_2} \tag{37}$$

The distribution of the interlaminar shear stress through the thickness can now be plotted and compared to results obtained by Pagano [3], as shown in Fig. 6. The solid line is the current solution, as represented by Eq.'s 36 and 37 respectively, whereas the circles represent the solution obtained by Pagano. Both solutions were obtained

for a span to thickness ratio of 4. As can be seen, the agreement between both solutions is excellent. The shear stress reaches a maximum at points A and C (Fig. 6.) in the 0° plies, which leads to the well-known cusp-like features in the shear stress distribution. The mathematical criterion for the occurence of a maximum within the 0° ply can be obtained by putting the derivative of Eq. 36 with respect to z equal to zero and by solving this equation for z. This procedure is demonstrated in appendix A.

It is very encouraging that the current solution-methodology enables us to obtain the detailed features of the interlaminar shear stress distribution. The interlaminar shear stress is matrix dominated and has a very damaging effect on the integrity of structural composite components. The obtained result is essential since this work is part of a larger program on durability of composites and wishes to incorporate the time-dependent aspects which are due to the matrix-dominated nature of these stresses.

Additionally, it has been shown that when tough thermoplastic-resin composites are impacted, most of the energy is dissipated through interlaminar shear deformtaion [4]. This again emphasizes the importance of this solution methodology for the design of impact resistant structures.

The distribution of bending stresses in the 0°/90°/0° laminate is obtained, using Eq. 16 combined with Eq. 36 (for the 0° ply) and Eq. 37 (for the 90° ply). The solid line in Fig. 7 was obtained using both formulas, whereas the circles represent the Pagano solution [3]. Excellent agreement is obtained.

By comparing Fig's 6 and 7 it can be seen that the corresponding locations, labeled A, B, C, in both figures coincide with two maxima and minima in the shear stress distribution. It is well known from the theory of strength of materials, that the bending stress at the neutral axis (point B) is zero, while the shear stress reaches a maximum. Strength of materials does not predict more than one maximum and is thus inapplicable for complex-multilayered composites which might have a number of maxima, proportional to the number of plies.

5.2 Modeling of Interleaves or resin-Rich Regions

Current methods to reduce the susceptibility of laminates to impact damage rely on the use of adhesive layers as interleaves . It was found [5] that these suppress impact-induced delamination, toughen the interface between two lamina and reduce matrix cracking.

The methodology outlines in this paper should serve well to guide in the optimal placement of adhesive layers to obtain the greatest benefit in improving impact resistance.

Consider a laminate, which consists of four 0° - plies, being subject to cylindrical bending. The loading conditions, geometry and material properties are same as for the example given in 5.1.

The interlaminar shear stress-distribution in the four-ply laminate was calculated using Eq. 17. The result is represented by the solid line in Fig. 8, whereas the circles represent results obtained by using Pagano's [3] solution methodology.

The introduction of three epoxy interleaves (E = .68 GPa or 10^5 psi and ν = .3) each of which only represents 3% of the total thickness drastically alters the shear-stress distribution as represented by the dotted line in Fig. 8.

As can be seen, the maximum shear stress, reached at the center of the laminate, is 33% higher than for the case of the ideal 4-ply composite. This might exhaust the shear-deformation capability of the epoxy and lead to failure. Interleaves are thus more effective to suppress impact when placed closer to the surface. The presence of resin rich area's also enhances the creep-characteristics of the laminate and reduces its buckling resistance. Both these features are currently being implemented into the methodology which we outlined in 2.

It can also be seen in Fig. 8 that the shear stress remains constant through the thickness of the interleaves. Consequently there will be discontinuities in the shear strains, because for shear modulus of the adhesive we used 1.37 GPa (.2 lb^6 psi), while the shear modulus of the plies was taken as 3.42 GPa (.510^6 psi).

5.3 Experimental-Theoretical Correlation for Thick Laminates Subject to Three-Point Bending

Post and coworkers [6] obtained interlaminar shear strain distributions on 48 ply laminates subject to three-point bending. This experimental data was obtained by means of a high-precision moire'-interferometry method. A schematic of the experimental setup and the dimensions is schematically shown in Fig. 9. A shear strain distribution was experimentally obtained along the line A-B, which is located at quarter span.

The analytical solution, which we obtained for the shear strain, using Eq. 17 can be written as:

$$\gamma_{xz} = \frac{2P}{a\ell h\, G_{13}} \sum_{1,3,5}^{\infty} \frac{\left(\frac{\cosh m\beta\ell z}{\cosh \beta\gamma_m} - 1\right)}{\left(1 - \frac{\tanh \beta\gamma_m}{\beta\gamma_m}\right)} \sin \gamma_m x \qquad (38)$$

All variables in Eq. 38 have been defined in section 4. The applied load is represented by P = 6120 N (1350 lbs). The thickness h = 12.78 mm (.5") and the span is 63.5 mm (2.5").

The material used was T300/5208, which has the following material properties:

$$E_{11} = 130 \text{ GPa } (19\ 10^6 \text{ psi})$$

$$G_{13} = 6.85\ (10^6 \text{ psi})$$

The series in Eq. 38 was evaluated for up to 200 terms. A comparison revealed that changes of less than 1% occurred after the first eight to ten terms. The resulting shear strain distribution is represented by the solid line in Fig. 10. The circles represent the experimentally measured strains. As can be seen, the obtained agreement is very good.

This agreement suggests a possible approach to obtain the interlaminar shear moduli G_{13} and G_{23}. First the analytical formula, Eq. 38 is used to determine the maximum shear strain at quarter span. This maximum shear strain is subsequently plotted for shear moduli ranging from 1.37 GPa (.2 MSI) to 13.7 GPa (2 MSI). The result is plotted in Fig. 11. It is now sufficient to mark the experimentally measured maximum strain on the ordinate and to read the corresponding

interlaminar shear modulus, G_{13} on the abcissa, as indicated by the arrows in Fig. 11. The value thus obtained for G_{13} is 6.23 GPa (.91 MSI). We should add that this is exactly equal to the value reported for T300/5209 by Sumsion and Rajapaske [7]. Data obtained by means of ultrasound measurements on T300/5208 [8] is the only other literature source we found and which lists a value of 7.12 GPa (1.04 msi) for G_{13}.

The approach should also work to determine the shear modulus G_{23}, which is often considered to be equal to G_{13} by the engineers who perform the finite element analysis. If indeed we would have made this assumption, to solve the problem for the 0°/90°/0° laminate in cylindrical bending, (see 5.11) the cusp-like features in the shear stress-distribu-tion (Fig. 6) would not have shown up, as discussed in appendix A.

The experimental results for T300/5208 and T300/5209 indicate that G_{23} is 44% and 49% lower than G_{13}. A difference of this magnitude is important enough to be considered for various design applications. Unfortunately the data is sorely lacking. Some data is available at room temperture, while none is available at elevated temperature. This conclusion is also true for the case of metal-matrix composites.

4.4 Load-Deflection Behavior of a Shear-Beam

Moussiaux et al. [9] recently published a paper on a new short-beam shear test specimen. The objective is to use the specimen for the shear characterization of an adhesive. The test-setup is schematically shown in Fig. 12.

Two aluminum adherends are bonded together with an adhesive. The methodology developed in [9] relates the overall deflection of the beam

methodology which we outlined in this paper can be effectively used to obtain results which are identical to these in ref [9]. We should add that the current approach is more general, because anisotropic adherends can be accounted for. It is also possible to locate the adhesive layer off-center and thus subject it to combined tensile and shear stresses.

The deflection at the free end of the beam is obtained by expanding the load P in Fourier series and by applying the summation procedure, discussed in section 4, to Eq. 33. This equation is in principle only applicable for the case of a single supported beam. The current results for a clamped beam were obtained by using the statically equivalent case of a single supported beam of twice the length and subject to twice the load.

Deflections were calculated for aluminum adherends (with E = 68. GPa or 10^7psi and ν = .3) and for varying properties of the adhesive. The length of the beam a = 63.5 mm (2.5"), the thickness of the adherends h_1 = 6.35 mm (.25") and the thickness of the adhesive was 7.27 mm (0.5"). The applied load was 445 N (100 lb).

First we calculated a reference deflection, W_{ref} assuming that the adhesive has the same properties as the adherends. (i.e. the deflection of a clamped aluminum beam which has a thickness of 13.97mm, (.55")).

Subsequently the adhesive was made more and more compliant and the calculated deflection of the beam consequently increased. this deflection was normalized with respect to the reference deflection.

The ratio W/W_{ref} has been plotted in Fig. 13 in which the abcissa is the ratio of young's modulus of the adherends (E) and the shear modulus of the adhesive (G_n). The solid line has been obtained using the methodology outlined in this paper. It was assumed that the

adhesive and the adherends have the same poissons ratio (ν = .3). The ratio E/Ga thus increases from 2.6, for the solid aluminum beam, to 10^6 for adherends which are basically no longer bonded. The triangles and the square symbols in Fig. 13 were obtained by Moussiaux et al. [9] and by using finite elements.

The deflection treshold, which is obtained for high E/Ga ratio's is reached because the very low stiffness of the adhesive allows the two adherends to act independently. A beam with unbonded adherends thus deflects about five times more than a solid aluminum beam.

This value for the deflection treshold can also be obtained on the basis of strength of materials. The reference deflection is given as:

$$W_{ref} = \frac{12Pa^3}{3E(2h_1 + h_2)^3} \tag{39}$$

The debonded beam can be pictured as two separate beams with a thickness h_1, each of which is acted upon by a load of P/2. We thus obtain:

$$W = \frac{\frac{P}{2} a^3}{3E \frac{h_1^3}{12}} \tag{40}$$

Dividing (40) by (39) we obtain:

$$\frac{W}{W_{ref}} = \frac{1}{2} \left(2 + \frac{h_2}{h_1}\right)^3 \tag{41}$$

Upon substitution of the numerical values for h_1 and h_2, we find

$$\frac{W}{W_{ref}} = \frac{1}{2} \left(2 + \frac{.05}{.25}\right)^3 = 5.32 \tag{42}$$

which is very close to the result obtained in Fig. 13.

Assuming that the adhesive was an epoxy with E = .68 GPa (10^5 psi) and ν = .3 we obtained the maximum shear stress in the adhesive layer as a function of the relative position along the beam, as plotted in Fig. 14. The circles represent the results obtained by Moussiaux et al. [9]. Again the agreement is excellent.

It is generally agreed upon that the interphase between the adherent and the adhesive needs modeling. The solutions which we presented are ideally suited to accomplish this task. Interphase regions which are only a few hundred angstrom thick can be easily accounted for because of our ability to derive analytical solutions there is no risk to run into mathematical problems or problems with computer algorithms. Precise solutions are guaranteed.

Results obtained by FIOR and Brinson [30] indicate that the use of deflection measurements on the shear beam cannot be used to determine the shear modulus of stiff adhesives. Instead, shear deformation measurements similar to the procedure discussed in section 5.3 have been recommended.

Notwhitstanding these comments, we further developed this procedure into dynamic regime, such that a simple frequency measurement defines the shear modulus of rigid as well as compliant adhesvies. These procedures are outlined in [11].

5. Conclusions

We demonstrated the use of simplified elasticity solutions, which lead to precise results for the displacements and the stresses in laminated composite beams and plates.

These solutions can be programmed on a simple hand calculator or on a PC. They can be used in the design office for preliminary sizing of structural composite and sandwich components subject to out-of-plane loads.

It was shown that excellent agreement was obtained with the much more cumbersome full-elasticity solutions for laminated plates. Special features, such as adhesive interlayers and resin-rich regions can be accounted for without additional complications. Excellent agreement was obtained with experimentally measured shear strains, obtained on a 48-ply laminated beam which was subject to three-point bending. This agreement led to the proposition of a new interlaminar shear modulus characterization test.

It was also shown that good agreement was obtained with results for the adhesive bonded shear beam. This opens the way to in-situ measurements of adhesive bondline properties.

The solutions which we discussed are useful to support and to advance a framework for durability predictions that has been proposed by Brinson [12]. More realistic constitutive equations, including hygrothermomechanical effects can be included by using the internal variable approach.

6. Nomenclature

$\varepsilon_x, \varepsilon_z, \varepsilon_{xz}$	strain-tensor components
$c_{11}, c_{13}, c_{33}, c_{55}$	coefficients of the stiffness matrix
$\sigma_x, \sigma_z, \tau_{xz}$	stress-tensor components
U,W	displacements in the x- and z-directions
M	stress-strain law coefficient (defined in Eq. (6))

ℓ	wavelength
q	transverse load distribution
β	dimensionless anisotropy factor (defined in eq. 17)
γ	dimensionless geometry factor (defined in eq. 17)
U_1, U_2	displacements along the top and bottom of a ply
τ_1, τ_2	interlaminar shear stresses at the top and bottom of a ply
P	transverse load
a	span
h	thickness of a ply (or laminate)
$E_L, E_T, \nu_{LT}, G_{LT}, G_{TT}$	material properties using the L-T notatin
$E_{11} E_{33}, \nu_{13}, G_{13}, G_{23}$	The same material properties, using the 1-3 notation

7. References

[1] Biot, M. A. "Mechanics of Incremental Deformations Wiley 1965

[2] Biot, M. A. "A New Approach to the Mechanics of Orthotropic Multilayered Plates" Int. J. Solids Structures, 1972, Vol. 8 pp. 475 to 490.

[3] Pagano, N. J. "Exact Solutions for Composite Laminates in Cylindrical Bending." J. Comp. Mat. Vol. 3, 1969 pp. 398-411.

[4] Williams J. G., "Effect of Impact Damage and Open Holes on the Compression Strength of Tough Resin/High Strain Fiber Laminates NASA CP 2334, 1983 pp. 61-79.

[5] Rechak, S. and Sun, C. T. "Optimal use of Adhesive Layers in Reducing Impact Damage in Composite Laminates" Composite Structures #4, I.H. Marshall, Editor, pp. 2.18-2.31, 1978.

[6] Post, D., Czarnek, R., Joh, D., Wood, J., "Deformation Measurements of Composite Multi-Span beam Shear Specimens by Moire' interferometry" NASA CR 3844 1984.

[7] Sumsion, T. H. and Rajapakse Y. D. S, "Simple Torsion Test for Shear Moduli of Orthotropic Composites" Proceedings ICCM/2, Noton, B. H. Editor, 1978, pp. 994-1002.

[8] Kriz, R. and Stinchcomb, W. "Elastic Modulus of Tranversely Isotropic Graphite Fibers and their Composites Experimental Mechanics 19 (1979) pp. 41-49.

[9] Moussiaux, E., Brinson, H. F. and Cardon, A. H., "Bending of a Bonded Beam as a Test Method for Adhesive Properties, VPI-E-87-9 Report, center for Adhesion Science, June 1987.

[10] Fior, V. F. and Brinson, H.F., "A Beam Test for Adhesives". Report #VPI-E-88-21, July 1988.

[11] Hiel, C. C. and Brinson, H. F. "An Improved Shear Beam Method for the Characterization of Bonded Composite Joints" Proceedings of the Society for experimental Mechanics '89 Spring Meeting (to be published).

[12] Brinson, H. F. "Durability (lifetime) Predictions of Adhesively Bonded Structures, Report # VPI-E-87-18. Center for Adhesion Science, July 1987.

8. Appendix A: Maximum Shear Stress in a 0°/90°/0° Laminate

As can be seen in Fig. 6, the shear stress reaches a peak in the 0° layer. Eq. 36 can now be used to derive an expression for the location of this peak the shear stress is maximum if

$$\frac{\partial \tau}{\partial z} = 0 \qquad (A.1)$$

Thus after subsitution of Eq. 36 into (A.1) we obtain

$$C_1 \sinh \beta_1 \ell z + C_z \cosh \beta_1 \ell z = 0 \qquad (A.2)$$

Solution of A.2 for z and substitution of the values for C_1 and C_2 defined in eq. 36 gives

$$z = \frac{1}{\beta_1 \ell} \tanh^{-1} \left[\frac{1}{1 + \frac{2\ell\, G_{13}}{\tau_2} W) \tanh \beta_1 \gamma_1} \right] \qquad (A.3)$$

Note that z lies in the domain $-\frac{h_1}{2}$ to $+\frac{h_1}{2}$.

The obtained value of z is a local coordinate measured to reference axes which are located at the center of the 0° ply, as indicated in Fig. A.1.

Eq. A.3 was used to determine the maximum shear stress in the 0°/90°/0° laminate, for a varying G_{23} modulus of the 90° layer. All other data used was the same as given in example 5.1. It was assumed that the laminate has unit thickness (thus each ply has a thickness of 1/3). Table A.1 contains the obtained results.

The negative signs in the solution for z mean that the maximum shear stress develops in that part of the 0° plies closer to the 0°/90° interface. It can be seen in the table that an increase in shear modulus G_{23} drives the maximum into the direction of the interface. This is made clearer in Fig. A.2, where we normalized G_{23} with respect to G_{13} (G_{13} = 5.10^6 psi). The vertical axis identifies the location of (τ_{xz}) max in % of $\frac{h_1}{2}$ (100% means the maximum is at the 0°/90° interface, 0% means the maximum is located at the center of the 0° ply).

As can be seen from the figure, the maximum shear stress will act at the interface for G_{23}/G_{13} ratio's larger than 7. A very low G_{23}/G_{13} ratio will force the 0° plies to act independently and force the maximum shear action at the center of each ply. The same reasoning applied to adhesively bonded beams, in which the adhesive changes properties due to environmental degradation and/or viscoelastic effects.

List of Captions

1. Orthotropic composite plate

2. Simple-supported orthotropic beam

3. Deviation between deflections obtained with strength of materials formulas and formulas outlined in this paper (for graphite epoxy material)

4. Cylindrical bending of 0°/90°/0° laminate.

5. Comparison of deflections for a range of span/thickness ratio's obtained using the current model (solid line) and Pagano's full elasticity solution (circles).

6. Comparison of interlaminar shear stresses, for span/thickness 4, obtained using the current model (solid line) and Pagano's full elasticity solution (circles).

7. Comparison of bending strains, for span/thickness = 4, obtained using the current model (solid line) and Pagano's full elasticity solution (circles).

8. Effect of interleaves on the interlaminar shear stress. Curve 1 line = no interleaves, Curve 2 = three interleaves.

9. Experimental setup and dimensions of a 48 ply 0° - deg T300/5208 laminate

10. Comparison of experimental (circles) and analytically (solid line) obtained shear strain distiributions at quarter span.

11. Variation of maximum shear strain, at quarter span, as a function of the shear modulus.

12. Setup and dimensions of short beam shear test specimen.

13. Deflection amplification for bonded shear beam for increasingly compliant adhesive.

14. Maximum shear stress in the bonded shear beam for various positions along the span. Comparison with solution by Moussiaux et al. (circles)

Appendix B

A.1 Detail of 0°-ply local coordinates

A.2 Position of the location of maximum interlaminar shear stress in the 0° ply

Table A.1.

(WP:mech-res)

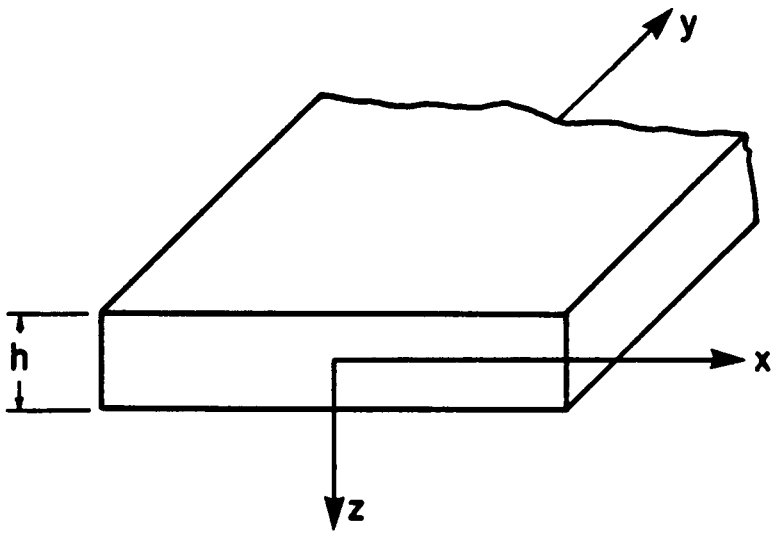

Fig 1

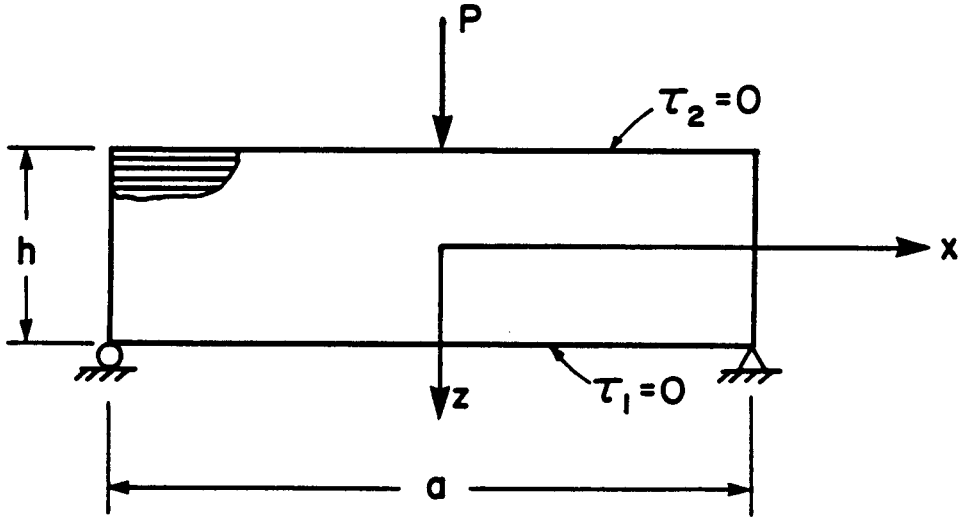

Fig 2

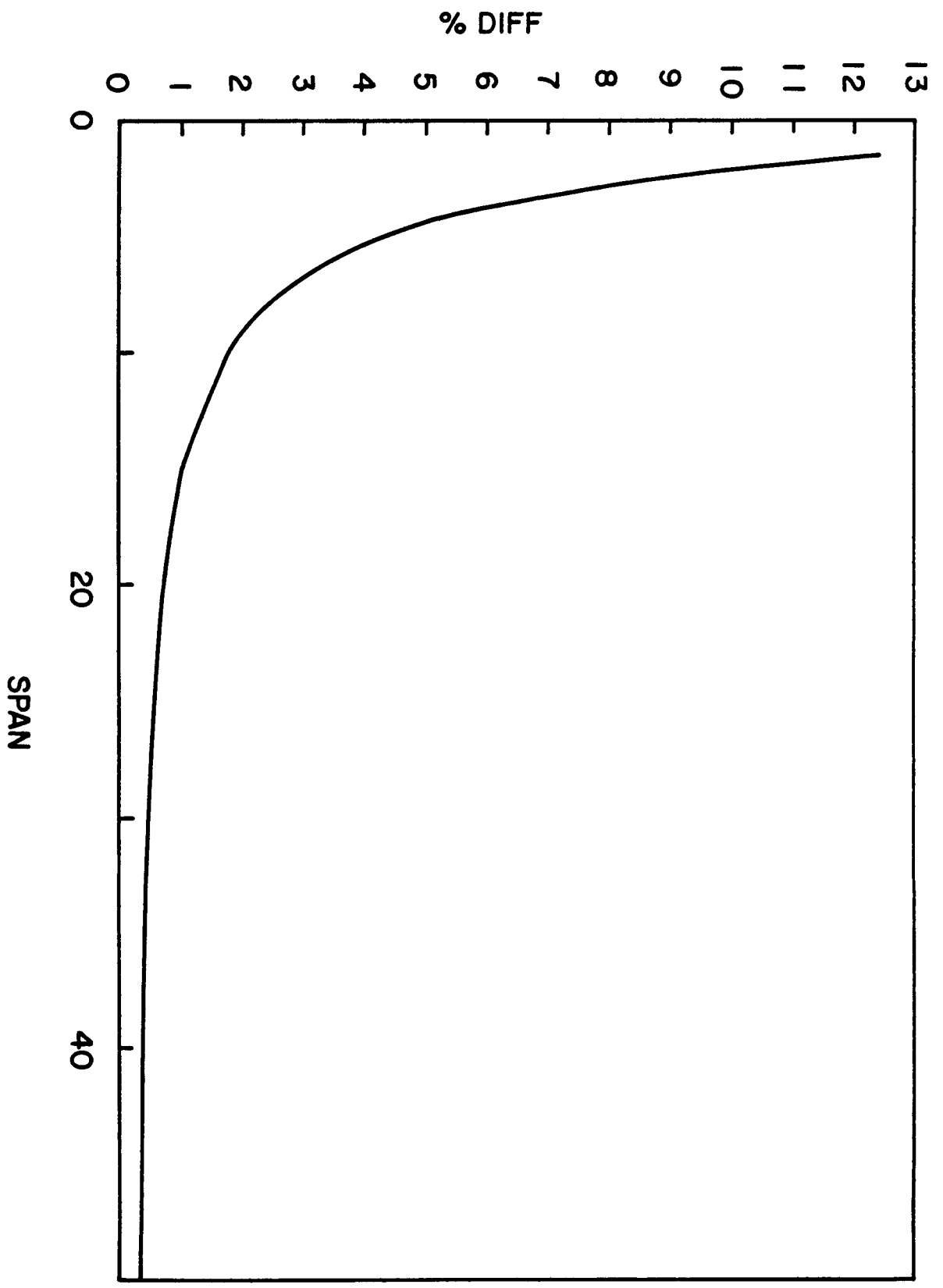

Fig 3

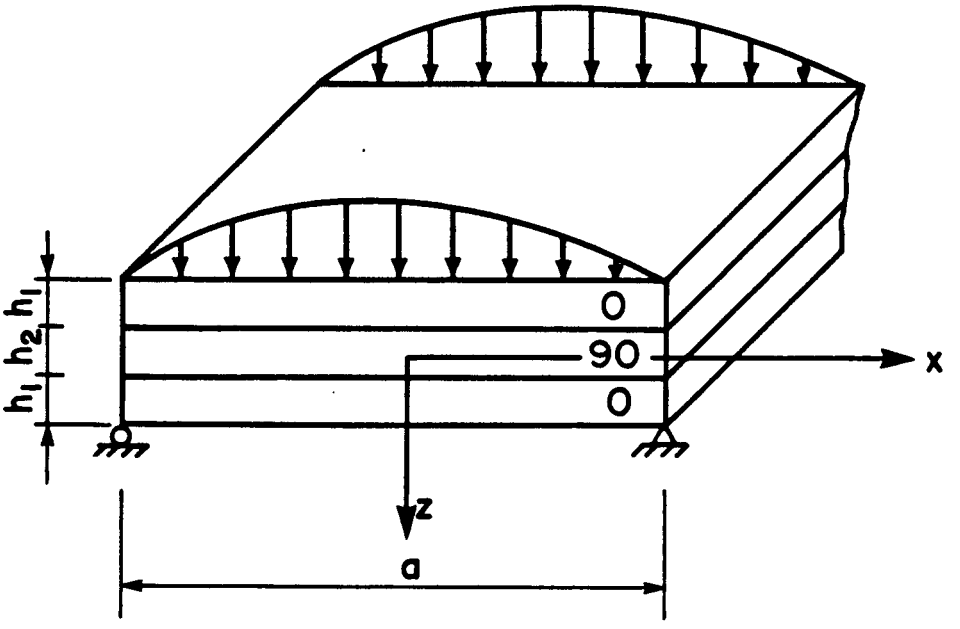

Fig 4

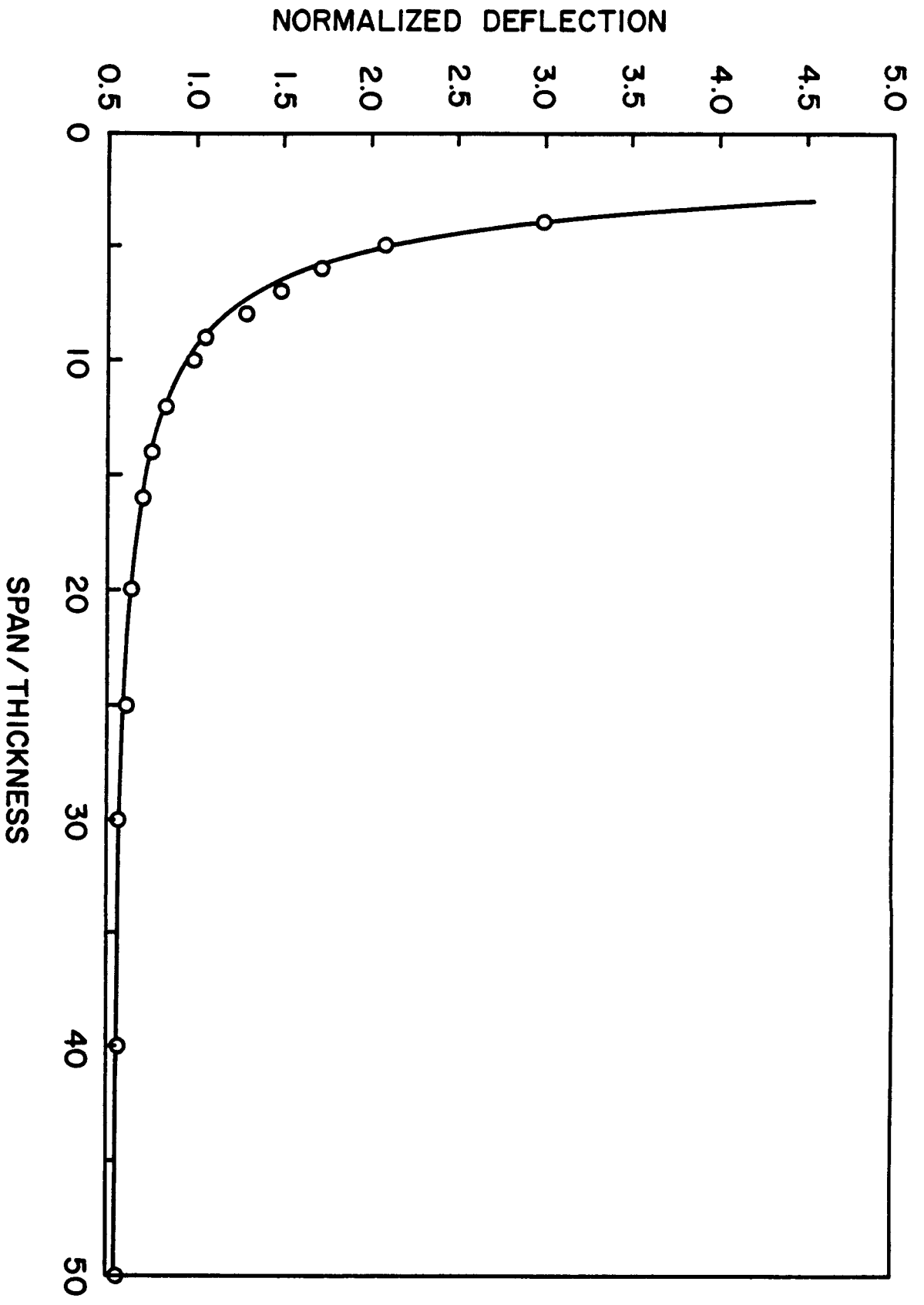
NORMALIZED DEFLECTION
0.5
1.0
1.5
2.0
2.5
3.0
3.5
4.0
4.5
5.0
SPAN / THICKNESS
0
10
20
30
40
50

Fig 5

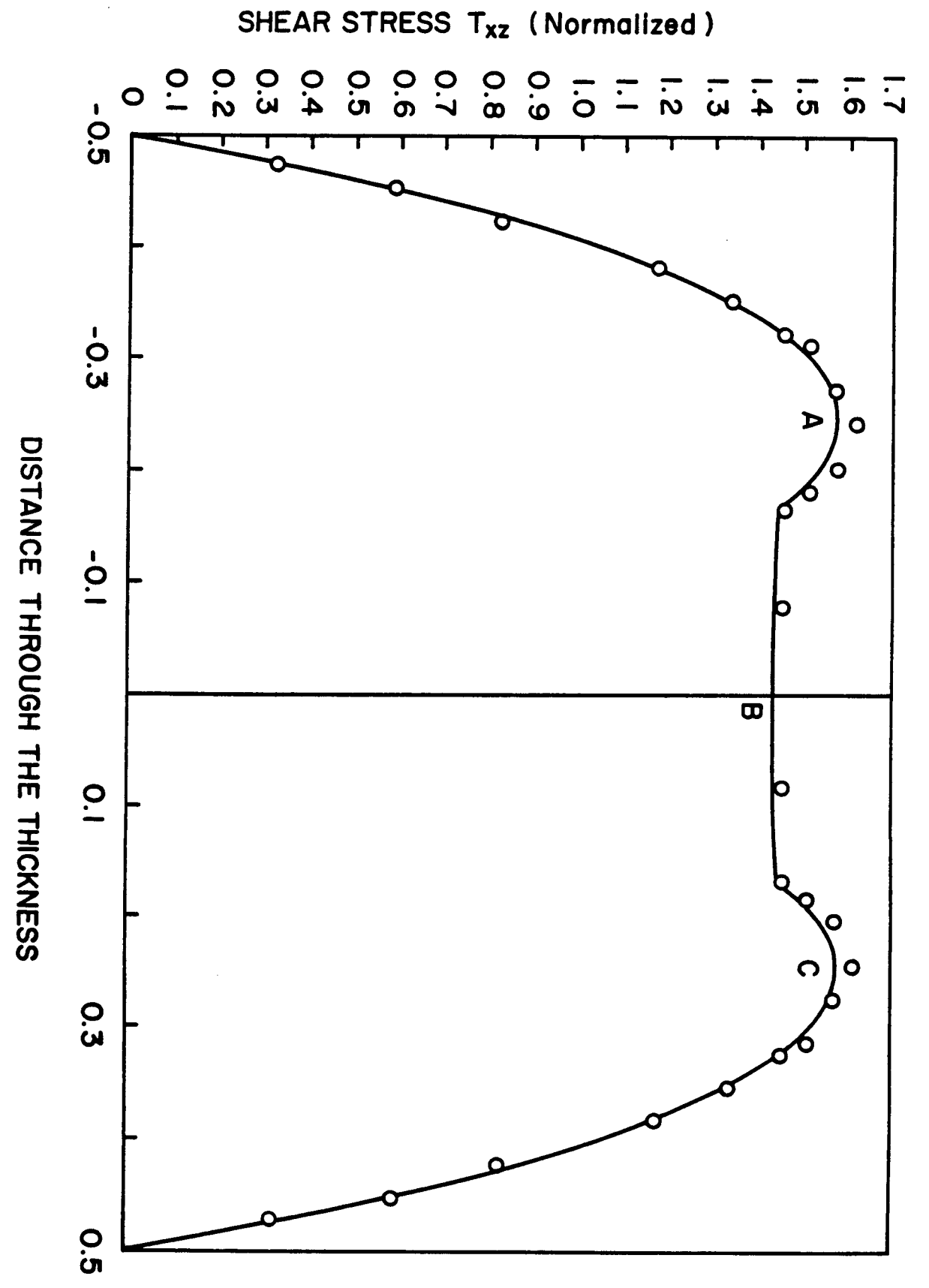
SHEAR STRESS T_{xz} (Normalized)
0
0.1
0.2
0.3
0.4
0.5
0.6
0.7
0.8
0.9
1.0
1.1
1.2
1.3
1.4
1.5
1.6
1.7
-0.5
-0.3
-0.1
0.1
0.3
0.5
A
B
C
DISTANCE THROUGH THE THICKNESS

Fig 6

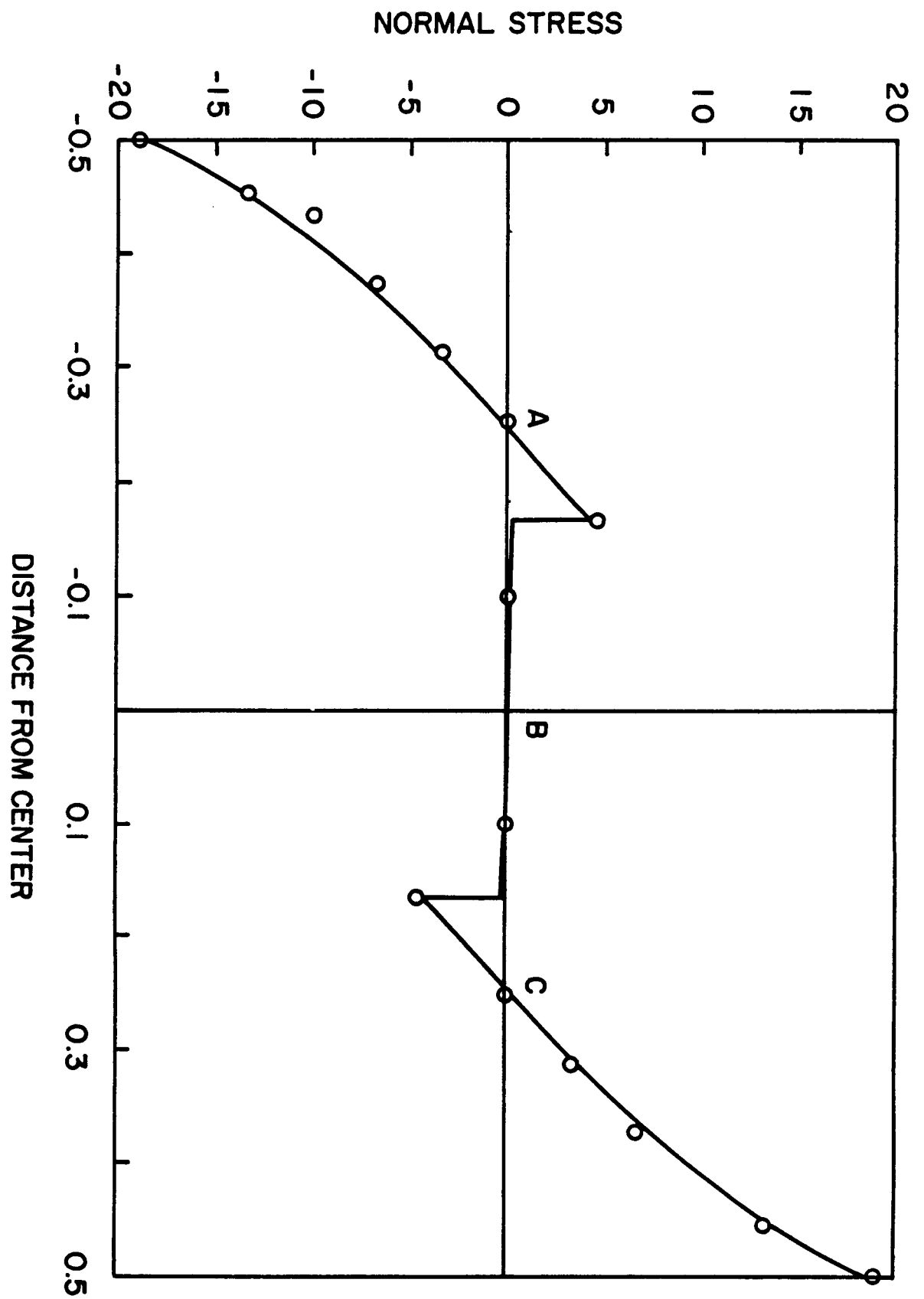
NORMAL STRESS
-20
-15
-10
-5
0
5
10
15
20
DISTANCE FROM CENTER
-0.5
-0.3
-0.1
0.1
0.3
0.5
A
B
C

Fig 7

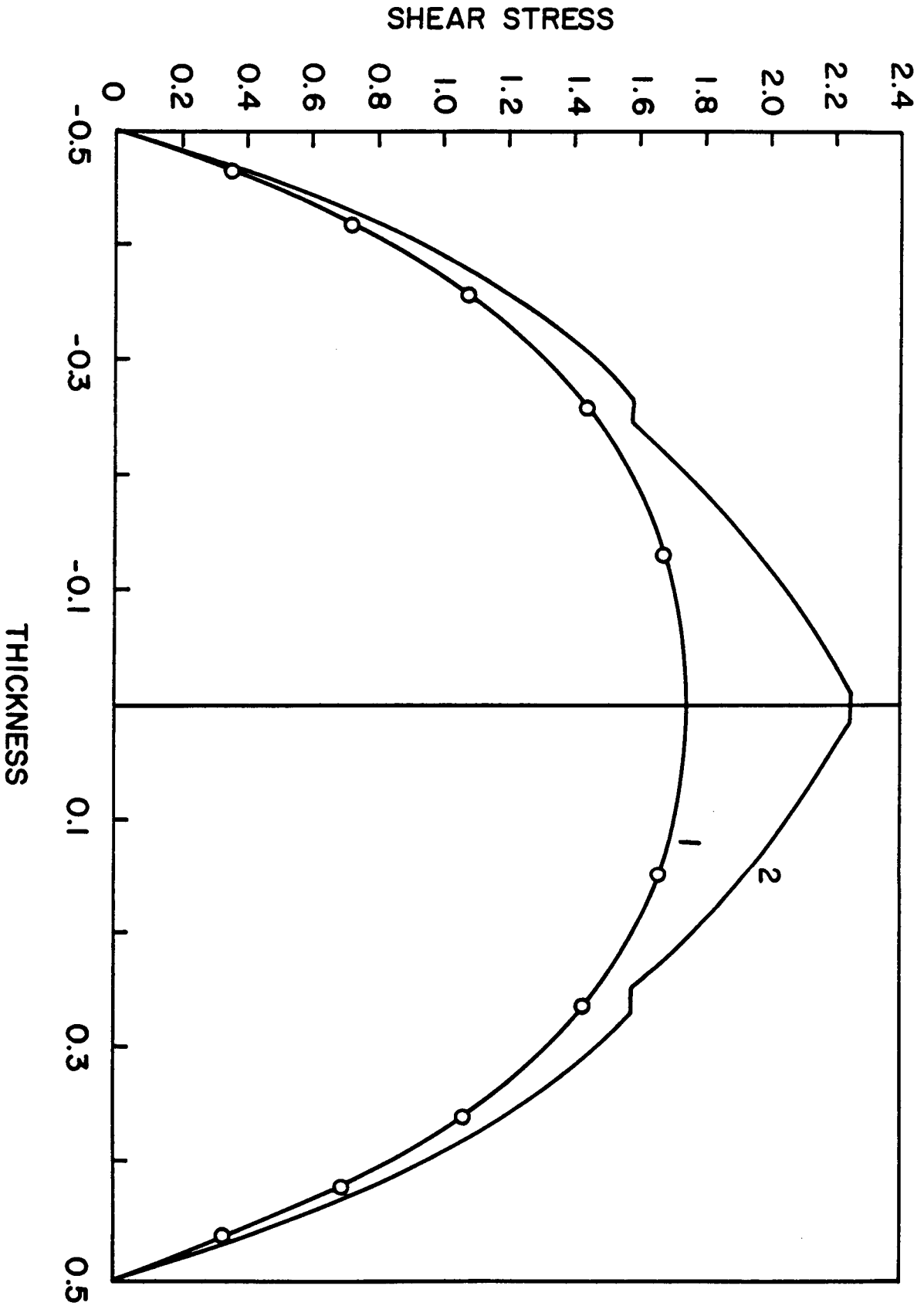
SHEAR STRESS
0
0.2
0.4
0.6
0.8
1.0
1.2
1.4
1.6
1.8
2.0
2.2
2.4
THICKNESS
-0.5
-0.3
-0.1
0.1
0.3
0.5
1
2

Fig 8

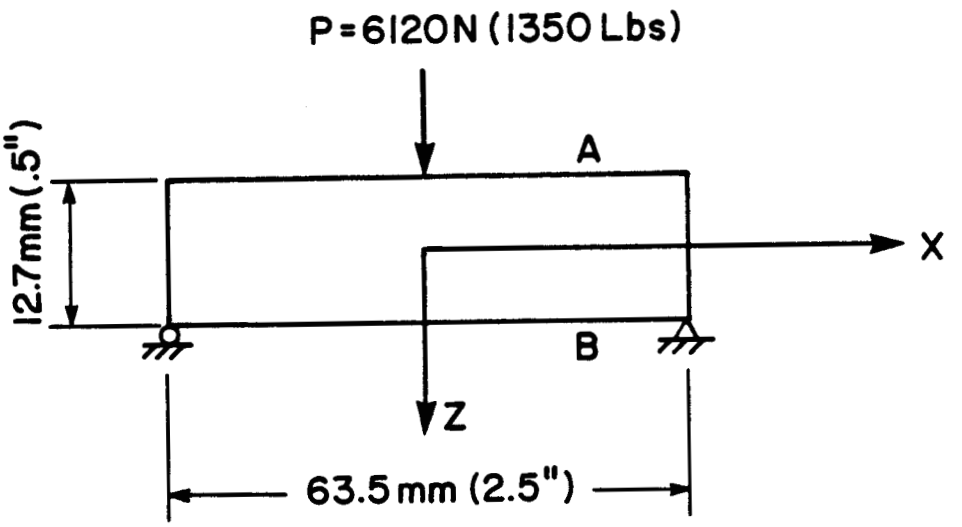

Fig 9

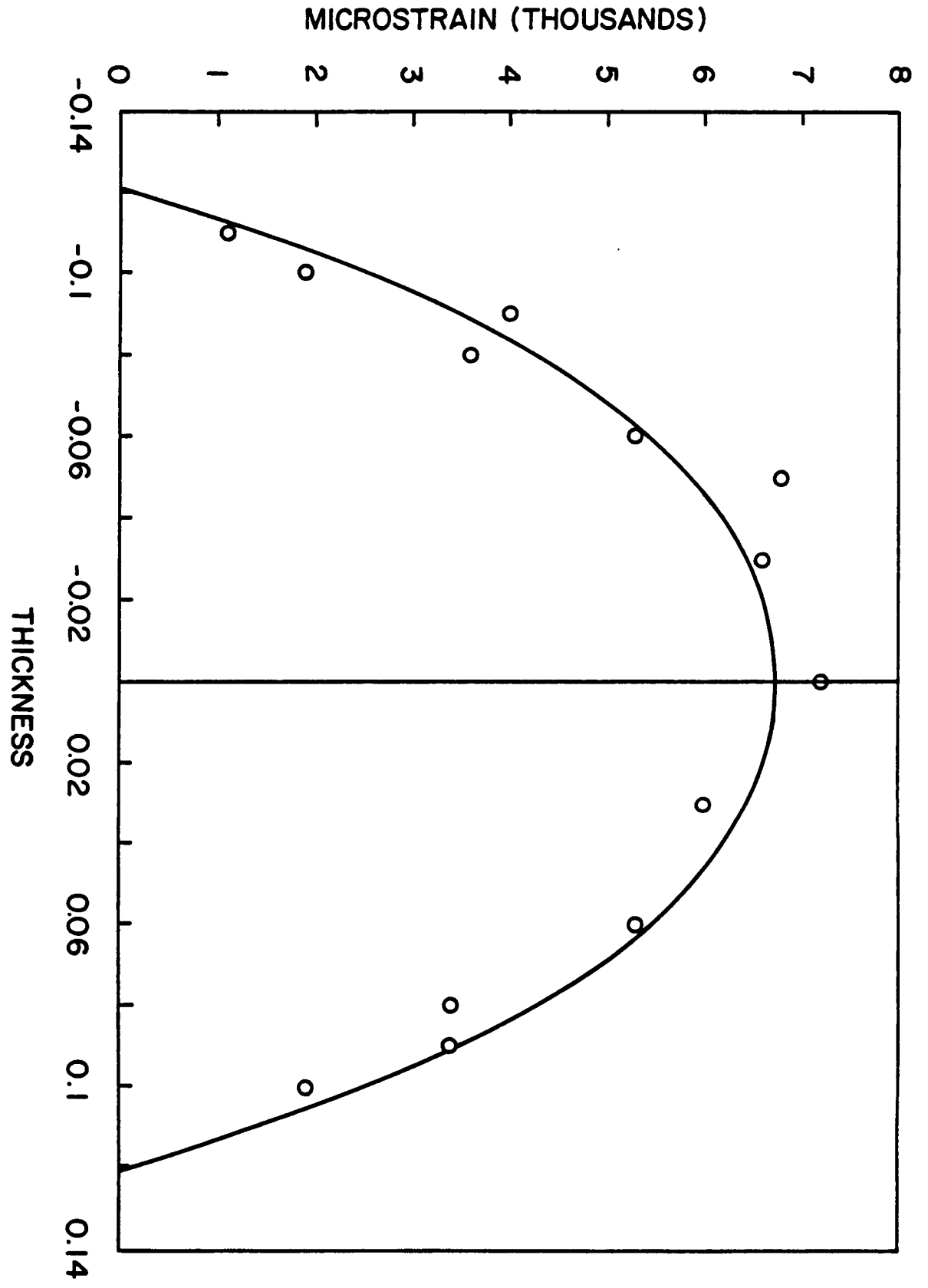
MICROSTRAIN (THOUSANDS)
0
1
2
3
4
5
6
7
8
THICKNESS
-0.14
-0.1
-0.06
-0.02
0.02
0.06
0.1
0.14

Fig 10

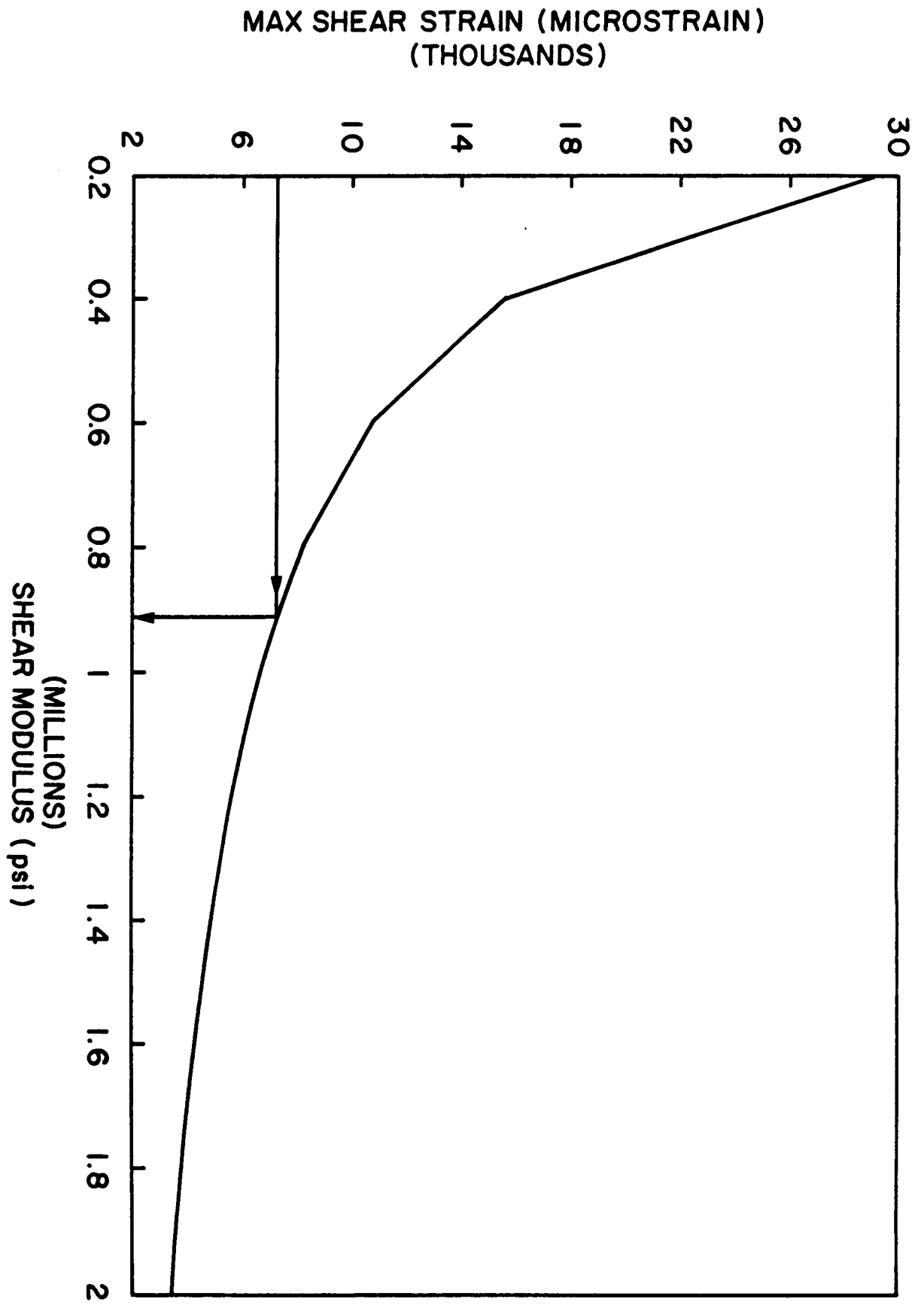
MAX SHEAR STRAIN (MICROSTRAIN)
(THOUSANDS)
2
6
10
14
18
22
26
30
0.2
0.4
0.6
0.8
1
1.2
1.4
1.6
1.8
2
(MILLIONS)
SHEAR MODULUS (psi)

Fig 11

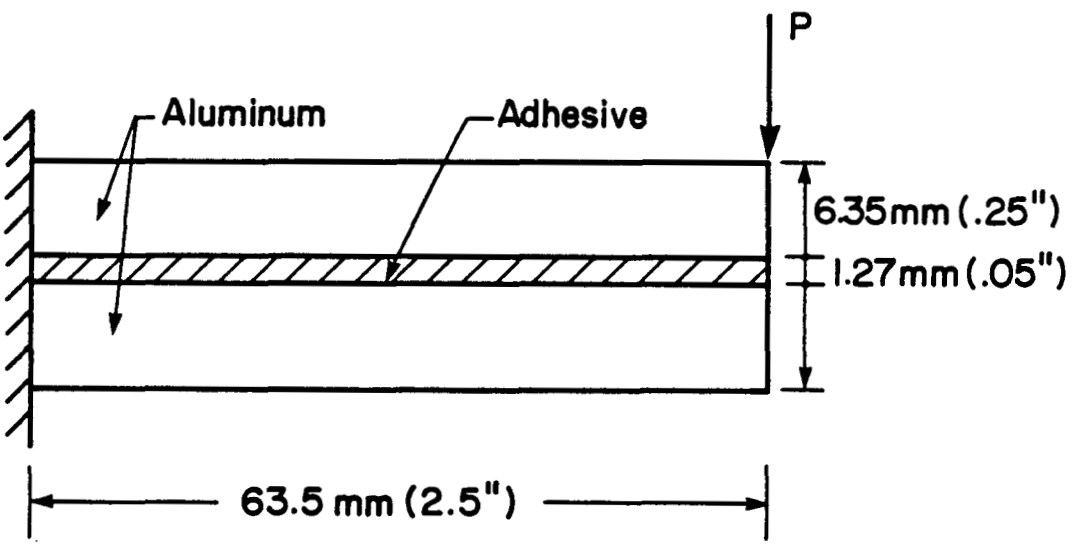

Fig. 2

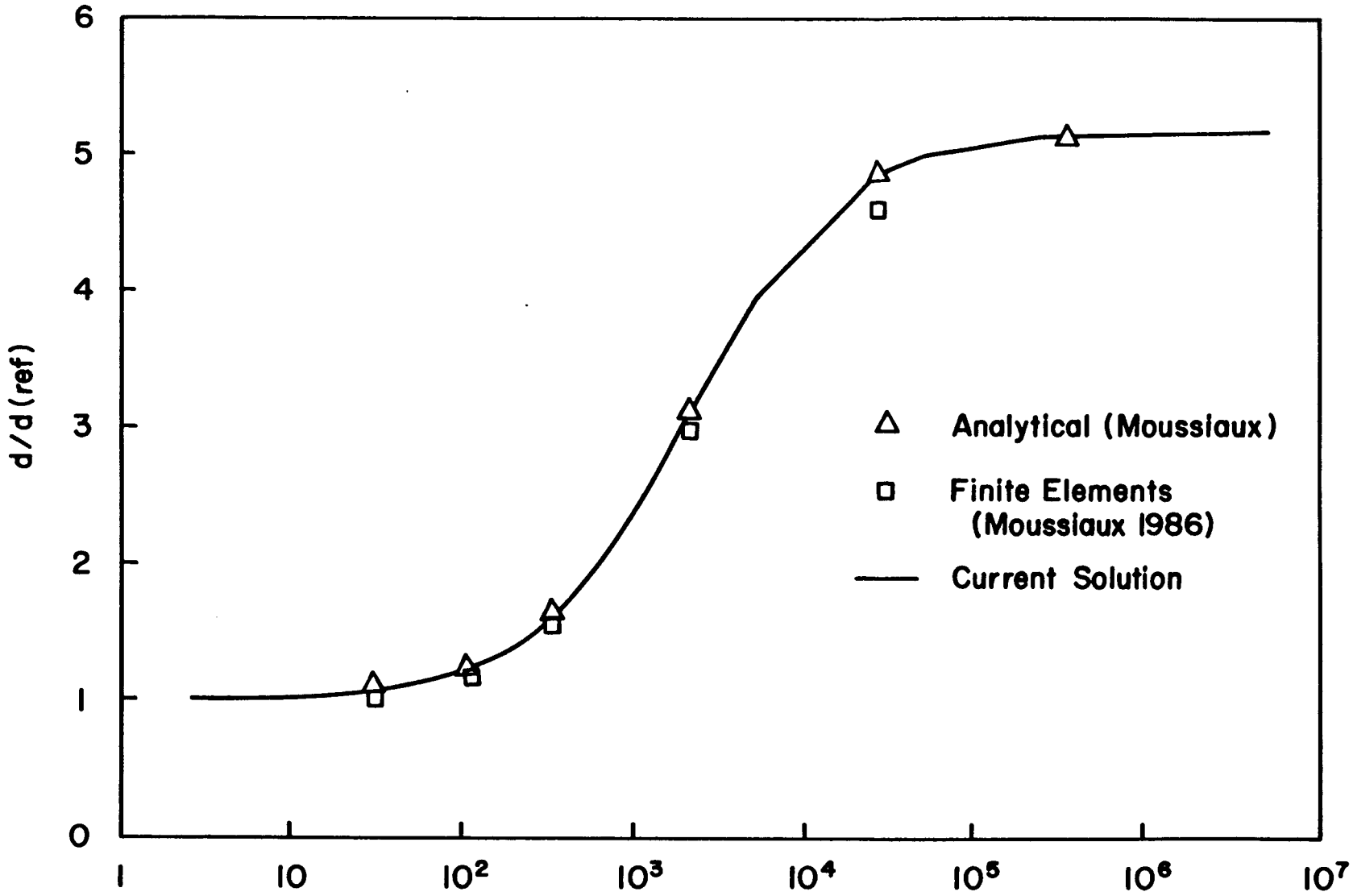
6
5
4
3
2
1
0
d/d(ref)
1
10
10^2
10^3
10^4
10^5
10^6
10^7
Analytical (Moussiaux)
Finite Elements
(Moussiaux 1986)
Current Solution

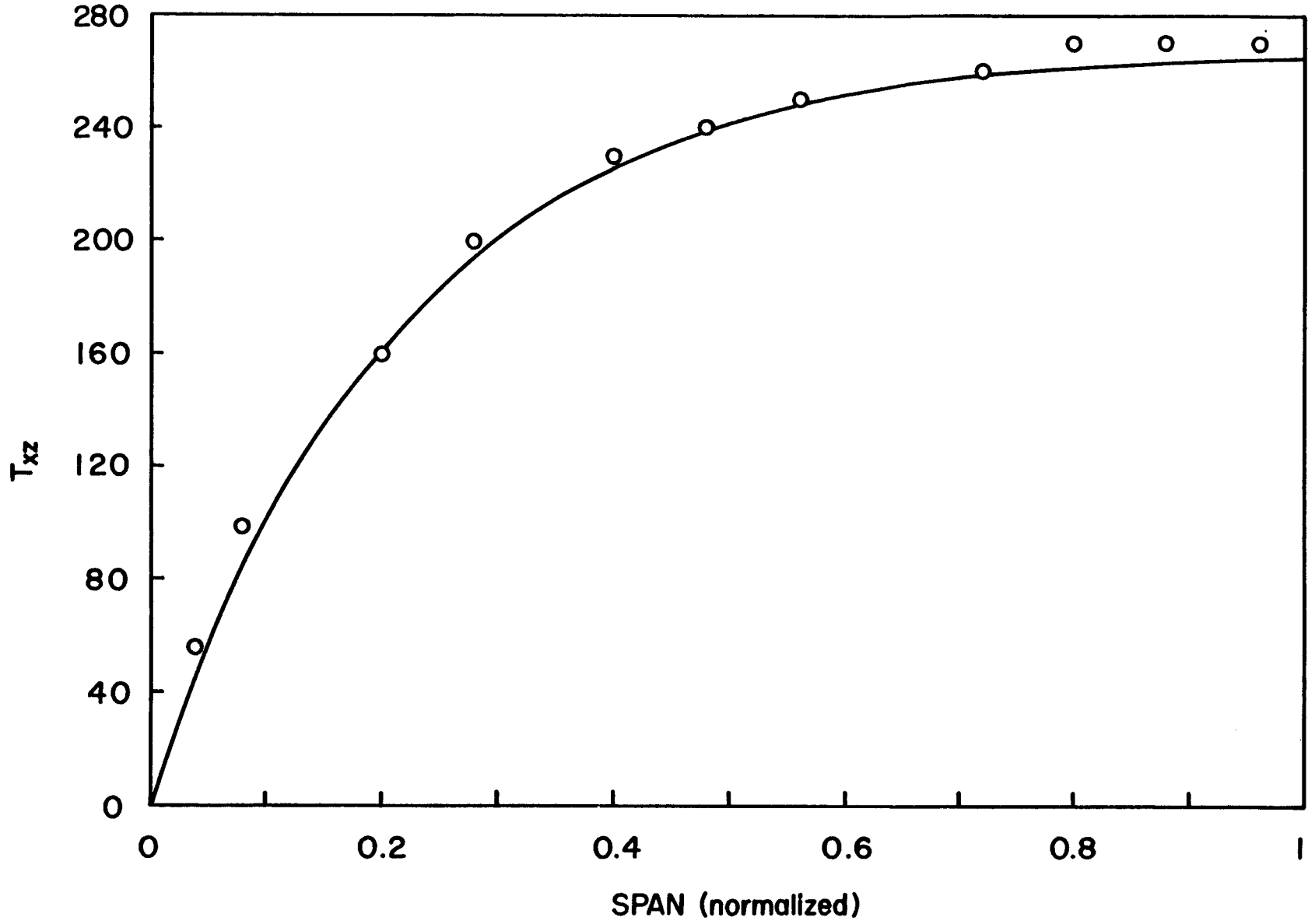
280
240
200
160
120
80
40
0
T_{xz}
0
0.2
0.4
0.6
0.8
1
SPAN (normalized)

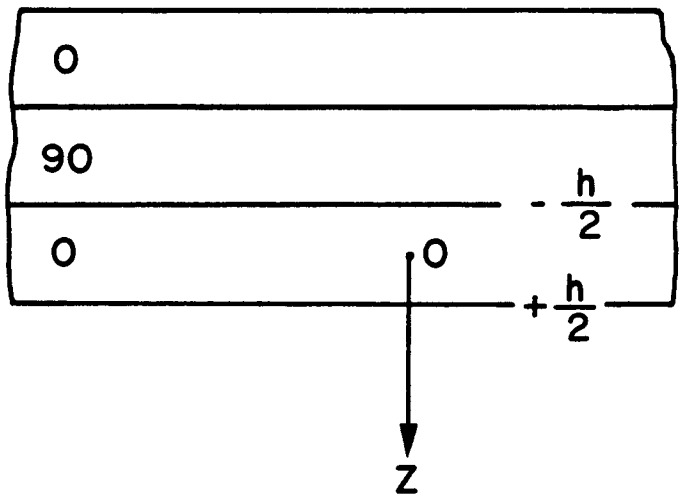
0
90
0
- h/2
0
+ h/2
Z

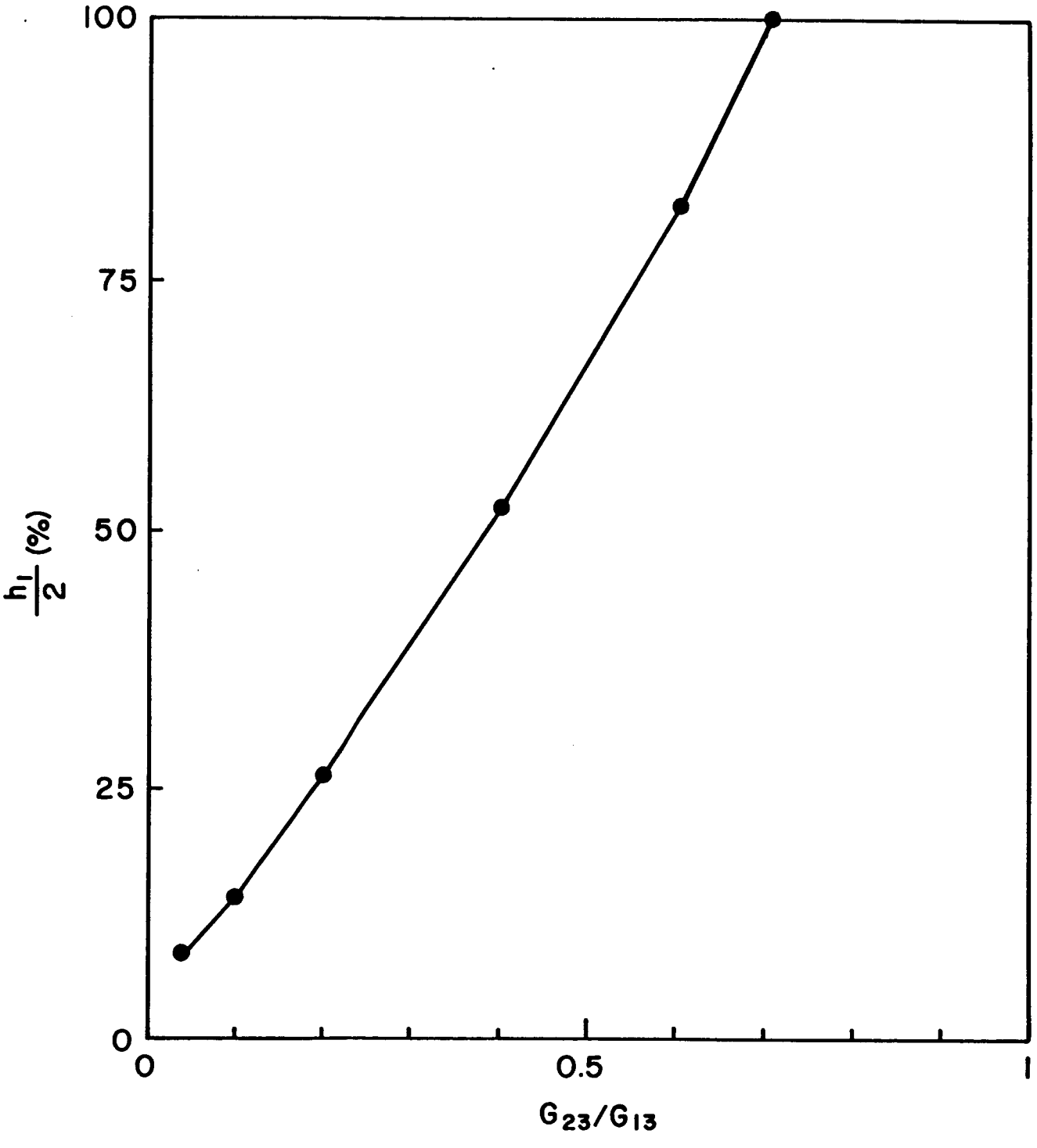
100
75
50
25
0
0
0.5
1
$\frac{h_1}{2}$ (%)
G_{23}/G_{13}